Two-photon laser scanning microscopy as a tool to study cortical vasodynamics under normal and ischemic conditions

Authors

A. Devor[1-3], A. Y. Shih[4], P. S. Tsai[4], P. Blinder[4], P. Tian[1], I. C. Teng[1] and D. Kleinfeld[4-5]

Institutional affiliations

[1]Department of Neurosciences, UCSD, La Jolla, CA

[2]Department of Radiology, UCSD, La Jolla, CA

[3]Martinos Center for Biomedical Imaging, MGH, Harvard Medical School, Charlestown, MA

[4]Department of Physics, UCSD, La Jolla, CA

[5]Graduate Program in Neurosciences, UCSD, La Jolla, CA

Summary

This review focuses on application of two-photon laser scanning microscopy (TPLSM) for *in vivo* imaging of vascular reactivity, neurovascular communication and as interventional tool for altering vascular and neuronal networks.

A mechanistic understanding of hemodynamics requires a systematic analysis of microvascular responses to changes in underlying neuronal activity. This analysis needs to be carried at the single vessel level in the context of the angioarchitecture of vascular networks (Scremin, 1995). Moreover, interventional strategies are needed to manipulate specific neuronal and vascular structures to test the role in neurovascular ensemble responses. In this context, recent advances in two-photon laser scanning microscopy (TPLSM) (Denk et al., 1990) allows one to measure the activity of single, visually-identified blood vessels with the potential for simultaneous measurements of neuronal and glial activity using calcium indicators (Stosiek et al., 2003; Ohki et al., 2005; Garaschuk et al., 2006), and targeted occlusion of single blood vessels (Nishimura et al., 2006; Schaffer et al., 2006; Nishimura et al., 2007). While technical aspects of TPLSM have been recently extensively reviewed (Denk et al., 1990; Denk and Svoboda, 1997; Svoboda and Yasuda, 2006), here we focus on the application of TPLSM to study cortical vascular dynamics under normal conditions and following experimentally-induced ischemic stroke.

Macroscopic imaging of blood oxygenation and flow

Great progress in understanding the relationship between different aspects of cerebral hemodynamics, such as blood flow, volume, and oxygenation, has been made through non-invasive macroscopic functional imaging methods: functional magnetic resonance imaging (Kwong et al., 1992; Ogawa et al., 1992), positron emission tomography (Fox and Raichle, 1986; Fox et al., 1988; Raichle and Mintun, 2006) and near infrared imaging spectroscopy (Villringer et al., 1993; Obrig and Villringer, 2003; Boas et al., 2004; Boas et al., 2004). These macroscopic methods can measure blood volume, oxygenation, and flow, but are unable to resolve individual vascular compartments: arterial, venous and capillary. In addition, all these methods have a limited spatial resolution, i.e., usually > 1 mm. Thus, physiological interpretation of these non-invasive

signals is based on numerous assumptions (Buxton et al., 1998; Davis et al., 1998; Mandeville et al., 1999).

Invasive optical imaging of “intrinsic signals” using a charge-coupled device (CCD) camera as a detector has been successfully used to map hemodynamic activity on a finer scale (Grinvald et al., 1986; Malonek and Grinvald, 1996; Vanzetta and Grinvald, 1999). Since oxy- and deoxyhemoglobin have different absorption spectra at visible wavelengths, intrinsic imaging provides a quantitative measure of hemoglobin oxygenation if two or more illumination wavelengths are used; the same principle is used by near infrared imaging spectroscopy (Malonek and Grinvald, 1996; Mayhew et al., 1998; Devor et al., 2003; Dunn et al., 2003; Devor et al., 2005; Dunn et al., 2005; Devor et al., 2007). Intrinsic imaging revealed a wealth of information regarding the relationship between blood oxygenation and volume (Berwick et al., 2002; Martindale et al., 2003; Sheth et al., 2003; Nemoto et al., 2004; Sheth et al., 2004; Sheth et al., 2004; Sheth et al., 2005) with inferences to blood flow and tissue metabolism (Vanzetta and Grinvald, 1999, 2001). Attempts have been made to isolate signals from major surface arteries and veins, and the capillary bed (Vanzetta et al., 2005). However, light scattering and lack of depth resolution, inherent to CCD-based methods, result in the contamination of signals by the surrounding tissue and introduce an ambiguity in interpretation.

A new technique, laminar optical tomography (LOT) (Hillman et al., 2004; Hillman et al., 2007), has been developed based on a combination of confocal illumination and an array of detectors collecting light at different distances relative to the illumination spot. Through modeling of photon migration, the general practice in diffuse optical methods (Boas et al., 2004), these distances are translated into cortical depths. Thus, LOT overcomes the lack of depth resolution by using calculated profiles of light penetration. LOT can also be used to estimate timecourses of oxygenation change across vascular compartments based on the signal timecourses isolated from major vessels (Hillman et al.,

2007). Nevertheless, similar to the CCD-based optical imaging of intrinsic signals, LOT suffers the effects of light scattering.

Laser Doppler flowmetry (LDF), which determines the speed of red blood cells (RBCs) from a shift in the frequency of reflected light, provides a point measurement of blood flow that can be serially repeated at multiple locations. LDF is accurate only for detecting relative changes since absolute measures of flux cannot be obtained (Dirnagl et al., 1989; Barfod et al., 1997). A scanning version of the LDF probe has also been implemented to obtain 2D images of flow (Lauritzen and Fabricius, 1995; Ances et al., 1999), as well as a recent interferometric method to simultaneously map flow across large area of cortex (Atlan et al., 2006). Laser speckle contrast imaging is an alternative method that allows 2D imaging of the flow. This method is based on the observation that the movement of RBCs through vessels will smear the speckle contrast when averaged over a short (~ 5 ms) time window (Dunn et al., 2001; Zhang and Murphy, 2007). Thus, both laser Doppler and laser speckle contrast imaging reflect the speed of RBCs, and a good correspondence between the two methods has been reported (Dunn et al., 2001). As other optical methods mentioned above, laser Doppler flowmetry and speckle contrast imaging do not resolve vascular compartments. In addition, a quantitative translation of these signals into blood flow requires a number of assumptions (Dirnagl et al., 1989; Dunn et al., 2001).

Microscopic *in vivo* imaging of vascular reactivity on the level of single blood vessels

The imaging techniques mentioned above average blood oxygenation or flow over large voxels (or pixels) of tissue including a multitude of small and large blood vessels. However, blood vessels that belong to different vascular compartments: arterial, venous and capillary, have different properties. Arterial vessels can actively change their diameter

and thus regulate blood blow since their walls contain smooth muscle cells, a substrate for active diameter control by neurovascular mediators; for a review see (Iadecola, 2004; Lauritzen, 2005; Hamel, 2006). The regulation of capillary diameter by contractile pericytes has also been demonstrated (Peppiatt et al., 2006). Veins, in contrast, do not possess active constrictive elements and passively comply with changes in pressure (Buxton et al., 1998).

The first serious attempt to study dynamics of single cerebral blood vessels was undertaken long before the invention of TPLSM (Wayland and Johnson, 1967). The investigators used a CCD detector to measure flow in surface capillaries based on movement of "void" segments with RBCs. Later, capillary flow was also observed using conventional fluorescence microscopy (Hudetz, 1997), and confocal laser scanning microscopy (Dirnagl et al., 1991; Villringer et al., 1994). Investigation of motion of RBCs in capillaries in superficial layers of rat cerebral cortex revealed a large variability in perfusion. However, a coherent response was observed following a hypercapnic challenge, measured as an overall increase in RBC flux (Villringer et al., 1994).

In contrast to confocal microscopy, TPLSM can image brain cortex up to 600 μm below the pia with micron resolution by using commercial low energy ultrafast laser oscillators (Kleinfeld et al., 1998), and up to 1000 μm with high-energy laser amplifiers (Theer et al., 2003). The depth penetration can be further extended *ex-vivo* using "all-optical histology" (Tsai et al., 2003), which complements TPLSM functional approach by providing complete reconstruction of underlying vascular architecture (**Figure 1**). All-optical histology takes advantage of the fact that ablation with ultrashort, near-infrared pulses is highly localized with minimal collateral damage (Tsai et al., 2003). Hence, it can iteratively image and ablate cortex to arbitrary depths while maintaining micrometer resolution and preserving the structural integrity of both the neurons and vessels.

The use of TPLSM to measure blood flow allows 3D mapping of evoked vascular response in single vessels across different vascular compartments (Chaigneau et al., 2007; Devor et al., 2007). TPLSM has been employed to image vascular changes in single vessels *in vitro* (Simard et al., 2003; Zonta et al., 2003; Cauli et al., 2004; Mulligan and MacVicar, 2004; Filosa et al., 2006; Rancillac et al., 2006) and *in vivo* (Faraci and Breese, 1993; Kleinfeld et al., 1998; Chaigneau et al., 2003; Takano et al., 2006; Chaigneau et al., 2007; Devor et al., 2007; Zhang and Murphy, 2007). The design of a two-photon laser scanning microscope has been described previously (Tsai et al., 2002).

Measurements of diameter and RBC speed describe blood flow in individual vessels

Two complementary measures, vascular lumen diameter and RBC speed, are used to characterize the vascular dynamics of an individual blood vessel. The lumen diameter of capillaries is small, i.e., < 10 μm in rat, and allows only single-file passage of RBCs. Capillary flow is typically only described in terms of RBC speed or flux, i.e., number of RBCs per second. In order to measure RBC movement *in vivo*, dextran-conjugated fluorescent dyes are injected intravenously to label the plasma (**Figure 2A**) leaving RBCs visible as dark shadows on bright fluorescent background (**Figure 2B**). The speed of the RBCs is captured by repeated line-scans along the axis of the vessel lumen that form a space-time image when stacked sequentially and leads to the generation of streaks caused by the motion of RBCs (**Figure 2C**). The speed of RBCs is given by the inverse of the slope of these streaks and the direction of flow is discerned from the sign of the slope. An algorithm based on singular value decomposition is used to automate the calculation of speed from the line-scan data (**Figure 2D-E**) (Kleinfeld et al., 1998).

In larger vessels, such as surface pial arterioles (**Figure 3A**), flow assumes a laminar profile with fastest flow in the center and slowest flow near the endothelial wall. Scanning is done along the central axis, where the speed is maximal (**Figure 3B**), and

RBC speed is also calculated from the inverse slope of the line-scan streaks (**Figure 3C**), as with capillaries. The average speed of RBCs in the arteriole is theoretically equivalent to one-half of the center-line speed, although this may be an underestimate for non-Newtonian fluids. The measurements from arterioles and capillaries typically show a periodic modulation due to the heart-beat (**Figure 3D**). The parabolic curve in **Figure 3E** represents the laminar flow profile (the fastest flow is in the middle of the vessel) that most closely matches the data.

Absolute vessel diameter is measured by obtaining a planar image stack, or by using continuous line-scans perpendicular to the vessel axis to gauge rapid changes over time (**Figures 4-5**). By scanning longer distances across multiple vessels, one can obtain the diameter changes of multiple vessels in a single space-time image (Devor et al., 2007). In this case, the scanning direction may not always be perpendicular to vessel axis for each of the measured vessels. However, the fractional diameter change is unaffected and the absolute diameter D can be obtained by $D = DM\sin(\theta)$, where DM is the measured diameter and the θ is the angle between the scan line and the axis of the vessel. In practice, the number of simultaneously measured vessels is limited to vessels in focus. One can overcome this limitation through development of more effective arbitrary line-scan algorithms (Gobel and Helmchen, 2007; Gobel et al., 2007).

By measuring both diameter and speed changes in the same arteriole, the vascular responses can be represented by flux, F, defined by $F = A*V$ where A and V is the cross-section area and average RBC speed, respectively. As mentioned above, the measurement of flux is unambiguous in capillaries since cells can only move single-file. For arterioles however, one can calculate flux as $F = (\pi/8)vd^2$, where v is the center-line speed and d is a diameter (Schaffer et al., 2006). While an increase in diameter or speed alone suggests but does not prove an increase in blood flow, e.g., an increase in diameter

can be accompanied by a decrease in speed, *F* gives a complete description of the vascular response at the time of measurement. **Figure 4** shows a comparison of diameter, RBC speed and flux in surface pial arterioles, penetrating arterioles, and capillaries. Despite the overlapping peaks in the diameter (**Figure 4A**) and speed (**Figure 4B**) profiles for the surface and penetrating arterioles, they differ significantly in flux (**Figure 4C**). The capillary profiles are also better separated from those of the arterioles with regards to flux.

Simultaneous measurements of neuronal and vascular activity

Two-photon laser scanning microscopy is strategically positioned to provide simultaneous measurements of the vascular and neuronal activity, crucial for understanding the basis of neurovascular coupling. In this respect, a study by our group (Devor et al., 2007) showed the spatial pattern of evoked diameter changes in surface arterioles as a function of distance from the focus of neuronal activity caused by somatosensory stimulation (**Figure 5**). Neuronal activity was not imaged simultaneously with vascular measurements, but was mapped prior to TPLSM. The results show that at every location within the exposure, arteriolar response was composed of an initial dilatory and later constrictive phase (**Figure 5A**). The relative strength of dilatation and constriction varied as a function of distance from the center of neuronal activity, where the strongest dilation was observed in the center and the strongest relative constriction was observed in the surround (**Figure 5B**). Moreover, these TPLSM findings were consistent with imaging of intrinsic signals and also with voltage-sensitive dyes (VSD) imaging. Comparison of TPLSM, intrinsic and VSD results demonstrated a correlation of the arteriolar constriction with enhanced neuronal inhibition. This study supports the hypothesis of neurogenic regulation of the arteriolar diameter, a key control parameter in the hemodynamic response (Cauli et al., 2004; Hamel, 2004, 2006; Rancillac et al., 2006).

While our study was focused on surface arterioles in order to facilitate the comparison with intrinsic optical imaging that has high sensitivity to the cortical surface (Polimeni et al., 2005), we expect that multiple parameters, such as vessel-type, distance from the center of neuronal activity and connectivity contribute to the vascular response. Ideally, mapping should be achieved by measuring individual penetrating arterioles. This is because surface arterioles are highly redundant and, as a result, have less specificity to cortical columns (Iadecola, 2004; Schaffer et al., 2006) than penetrating arterioles that feed well-defined columns of cortical tissue (Nishimura et al., 2007).

Neuronal activity can be imaged simultaneously with measurements of vascular dynamics and RBC speed by using calcium indicators (Chaigneau et al., 2007) (**Figure 6**). A study by Chaigneau et al. investigated the relationship between the capillary blood flow and neuronal activity in the olfactory bulb *in vivo* using extrinsic calcium dyes in rats and genetically-encoded indicators in mice (Chaigneau et al., 2007). In rats, calcium indicator Oregon Green BAPTA-1 was loaded into mitral cells in the olfactory glomeruli intracellularly through a recording pipette, while in mice transgenic expression of G-CaMP2 served as the indicator (Diez-Garcia et al., 2005). In all experiments, blood plasma was labeled by intravenous injection of Texas Red dextran. The authors observed an increase in capillary RBC speed concurrent with an increase in calcium in dendritic branches of mitral cells following an odor stimulus (**Figure 6**). This study demonstrated the feasibility of simultaneous imaging of neuronal calcium signals and capillary RBC speed using TPLSM. Furthermore, it supports the prior hypothesis that neuronal intracellular calcium concentration plays a central role in neurovascular coupling (Lauritzen, 2005).

An ability to image both neuronal and glial calcium transients is important for neurovascular research since both neurons and glia have been implicated in communication to the vasculature (Cauli et al., 2004; Mulligan and MacVicar, 2004; Rancillac et al., 2006; Takano et al., 2006; Chuquet et al., 2007). Further, functional

changes in calcium levels can also be detected in arteriolar smooth muscle, which appear to coincide with active changes in vascular diameter (Filosa et al., 2004). Therefore, through a combination of calcium imaging and direct blood flow measurements, TPLSM can be used to observe neurons, glia, and vessels that control blood flow. This approach is expected to aid the identification of cellular elements that control vascular response under normal conditions and possibly the mechanisms that lead to its failure during pathology.

TPLSM as an intervention tool

Two-photon laser scanning microscopy can be used not only to image neuronal and vascular activity but also to manipulate neuronal circuits and vascular architectonics *in vivo*. Nishimura et al. have developed a method for targeted occlusion of single capillaries deep to the cortical surface by using two-photon irradiation (Nishimura et al., 2006). This method makes use of plasma-mediated ablation through the nonlinear absorption of 100-fs, ultrashort laser pulses by blood plasma or the vascular wall, generating a variety of injury models including intravascular clots, serum extravasation, and hemorrhage. Another method for targeted occlusion of single vessels is based on focal photothrombosis induced by optical activation of the photosensitizer Rose Bengal (Schaffer et al., 2006; Nishimura et al., 2007; Sigler et al., 2008). Unlike the use of nonlinear absorption, photothrombotic clots are confined to the cortical surface since irradiation of Rose Bengal dye is performed with a green laser. A recent study demonstrated that photothrombic occlusion of localized middle cerebral artery branches is sufficiently accurate to remove targeted regions of the somatosensory representation while leaving neighboring regions intact (Zhang and Murphy, 2007). Similarly, the authors used this method to demonstrate that surface arterioles form complicated redundant interconnected networks (Schaffer et al., 2006), and therefore can tolerate a local damage, while penetrating arterioles define only partially

overlapping vascular territories (**Figure 7A)** (Nishimura et al., 2007). **Figure 7** gives an example of single penetrating arteriole occlusion and illustrates the loss of flow in downstream microvessels and the resultant generation of a column of hypoxic tissue (**Figure 7B)**.

In future studies, TPLSM will also be used for targeted ablation of neurons. A body of recent data increasingly suggests that differential vascular control originates from activation of specific neuronal sub-populations through release of specific vasoactive agents (Cauli et al., 2004; Hamel, 2004, 2006; Rancillac et al., 2006). However, direct evidence showing that selective activation of known cell types correlates with vasodilation or vasoconstriction *in vivo* is missing. Ablation of single or multiple neurons with known vasoactive properties can be used to test the spatial precision of neurovascular control. In principle, TPLSM can also be used for activation of single cells. Selective *in vivo* photoactivation has been achieved by use of the light-gated ion channel Channelrhodopsin-2 (Arenkiel et al., 2007), that exhibits a nonselective cation flux when exposed to blue-green light (Sineshchekov et al., 2002; Nagel et al., 2003; Boyden et al., 2005). This and other recently developed methods for targeted photoactivation (Han and Boyden, 2007; Szobota et al., 2007; Volgraf et al., 2007; Zhang et al., 2007) in current practice require one-photon excitation. Thus, the excitation cannot be limited to a single cell. In future, similar agents will be developed amendable to TPLSM.

Conclusions

Multiple parameters, such as vessel-type, distance from the center of neuronal activity and connectivity, contribute to the vascular response. Although putative regulatory structures has been identified in *ex vivo* corrosion casts (Harrison et al., 1998), measurement of both diameter and RBC speed across vascular compartments and cortical depths are needed to address the question of spatial precision of the vascular

functional control *in vivo*. Recent developments in TPLSM and optical probes have greatly advanced our understanding of relationship between the activity of neuroglial control elements and resultant vascular changes. Further technological developments are needed to estimate currently unknown variables such as intravascular blood pressure, shear stress, blood and tissue gas (O_2, CO_2, and NO) and pH, which are required for mechanistic modeling of neurovascular dynamics.

Figure Legends

Figure 1. Reconstruction of mouse cortical vasculature. The mouse cortical vasculature was labeled using a fluorescent perfusion cast. The surface vascular network includes pial arteries, arterioles, and veins, while the subsurface vasculature consists of dense capillary beds. Penetrating arterioles, one of which is shown in yellow, bridge the flow of blood from surface to subsurface vessels. The entire cortical thickness was imaged using iterations of TPLSM followed by laser ablation of the imaged tissue depth, i.e., all optical histology (Tsai et al., 2003).

Figure 2. Measurement of lumen diameter and RBC speed of individual capillaries. (A) Projection of TPLSM image stack showing subsurface capillaries labeled with fluorescein-dextran dye *in vivo*. The capillaries were 300-400 μm below the cortical surface. The *inset* shows the intensity profile along the cross section for the capillary in question. The lumen diameter is estimated from the number of pixels with intensity above the background level. **(B)** Successive planar images through a capillary, acquired every 16 ms. The change in position of an unstained RBC against a fluorescent background is indicated by the series of arrows; the speed of the RBC is +0.11 mm/s. **(C)** RBC speed was calculated from line-scans collected repeatedly along the central axis of the capillary, which were then stacked sequentially to form a space-time image. The streaks within the line-scan are caused by unstained RBCs moving through the capillary over time. The x-axis represents the distance traveled by the RBCs (x) and the y-axis represents time (t). RBC speed is then calculated from the inverse of the slope of the RBC streaks ($\Delta t/\Delta x$); the direction of flow is discerned from the sign of the slope. **(D)** Illustration of automated algorithm for finding slope of streaks formed by moving RBCs. Line-scan data from an epoch in time is transformed to a square matrix with normalized axes. In the left image, an abrupt change in the slope of the streaks can be due to a heartbeat or irregularity in capillary flow. The central region of the square matrix is rotated to find the angle that yields horizontal streaks, as in the middle panel (arrowhead). **(E)** Separability of line-scan data as a function of rotation angle; separability is maximal for vertical or horizontal streaks. Figure adapted from Kleinfeld *et al.* (1998).

Figure 3. Measurement of RBC speed of individual pial arterioles. (A) Low-magnification TPLSM image of pial vessels in rat cortex labeled with fluorescein-dextran dye *in vivo*. The axes indicate the rostral (R) and medial (M) directions. **(B)** Maximal

projection of a TPLSM image stack through a surface arteriole identified in the inset in (A). The dark line indicates the location where the line-scan data were taken, and the arrow represents the direction of flow obtained from these scans. **(C)** Line-scan data from the vessel in (B) to quantify RBC speed. As with capillaries, RBC speed is measured from the inverse slope of the line-scan streaks; see Figure 2C-2E. **(D)** RBC speed along the central axis of the arteriole shown in (B) and (C) as a function of time. The periodic modulation of the RBC speed occurs at the approximately 6-Hz heart rate. The dotted line represents the temporal average of the speed. **(E)** The speed of RBCs in a different arteriole, averaged over 40 s, as a function of the transverse position in the vessel along horizontal (y) and vertical (z) directions. The parabolic curve represents the laminar flow profile that most closely matches the data. Figure adapted from Schaffer *et al.* (2006).

Figure 4. Quantitative blood flow measurements from individual cerebral pial arterioles and capillaries. Compendium of *in vivo* measurements including lumen diameter **(A)**, average RBC speed **(B)**, and volume flux **(C)**, collected from three distinct vessel types of the rat cortex. For penetrating arterioles, RBC speed was measured at locations where the vessels were oriented in xy plane. Arteriole flux was calculated using the equation $F = (\pi/8)vd^2$, where v is the center-line RBC speed and d is the lumen diameter. For capillaries, flux was calculated using the same equation minus a laminar flow constant, $F = (\pi/4)vd^2$. Arteriole data was taken from Shaffer *et al.* (2006) and Shih *et al.* (unpublished). Capillary data is from Kleinfeld *et al.* (1998). Surface arterioles (n = 454), penetrating arterioles (n = 360), and capillaries (n = 35).

Figure 5. TPLSM imaging of vascular response to a somatosensory stimulus. (A) Stimulus-evoked diameter changes in single arterioles. Increase in the diameter is plotted upward, and decrease is plotted downward. Electrophysiological response to the stimulus was mapped using a ball electrode. Recorded surface potentials (red traces) are overlaid on the image of the brain surface vasculature. Both vasodilatation and vasoconstriction are present at all locations. The degree of vasodilation decreases with an increase of distance from the center of neuronal activity, denoted by the largest surface potential amplitude. **(B)** Initial vasodilation in vascular diameter time-courses is normalized. Area with the largest neuronal response (red traces in A) is denoted by a red circle. This area corresponds to the center of the evoked neuronal activity. Note that vasoconstriction increases with an increase in distance from the center.

Figure 6. Simultaneous TPLSM imaging of the capillary blood flow and neuronal activity in the olfactory bulb. A single mitral cell was labeled with calcium indicator Oregon Green BAPTA-1 through an intracellular pipette and imaged with TPLSM. Odor stimulus (hexanal 1.2%) generated calcium increases in the dendritic tuft and RBC speed increase in a nearby capillary. Calcium measurements were performed using line-scan acquisition, allowing simultaneous measurement of RBC speed. Red triangles under RBC speed time-course indicate times corresponding to blood flow recordings shown on the right. Figure adapted from Chaigneau *et al.* (2007).

Figure 7. Photo-thrombotic occlusion of penetrating arterioles using Rose Bengal. (A) Projected TPLSM image of a single penetrating arteriole occluded by photo-thrombosis (yellow circle) shown in the coronal plane (X-Z maximal projection), with surface arterioles near the top of the image. For the same field of interest, the surface vascular network is visible in the plane tangential to the cortical surface (X-Y maximal projection). The RBC speed in two neighboring surface vessels (Vessel 1 and 2) was measured using repeated line-scans. Vessel 1 shows no change in post-occlusion RBC speed (v_{post}) compared to baseline (v_{base}), whereas Vessel 2 shows essentially no flow after the occlusion. **(B)** Examination of the hypoxic volume generated after a single penetrating arteriole was occluded (yellow circle). Pimonidazole hydrochloride (Hypoxyprobe^{TM}) was injected intravenously after clot formation and 1 h before transcardial perfusion. To locate the occluded vessel after brain extraction, fiducials markers were electrolytically placed near the target vessel before the brain was extracted from the skull. The ipsilateral cortex was then removed and flattened prior to immunohistology. Pimonidazole staining revealed a column of hypoxia, within the dashed yellow circles, that reached 700 μm below the pial surface. Panel A and B were adapted from Nishimura *et al.* (2007) and Kleinfeld *et al.* (2008), respectively.

References

Ances BM, Greenberg JH, Detre JA (1999) Laser doppler imaging of activation-flow coupling in the rat somatosensory cortex. Neuroimage 10:716-723.

Arenkiel BR, Peca J, Davison IG, Feliciano C, Deisseroth K, Augustine GJ, Ehlers MD, Feng G (2007) In vivo light-induced activation of neural circuitry in transgenic mice expressing channelrhodopsin-2. Neuron 54:205-218.

Atlan M, Gross M, Forget BC, Vitalis T, Rancillac A, Dunn AK (2006) Frequency-domain wide-field laser Doppler *in vivo* imaging, Optics Lett 31:2762-2764

Barfod C, Akgoren N, Fabricius M, Dirnagl U, Lauritzen M (1997) Laser-Doppler measurements of concentration and velocity of moving blood cells in rat cerebral circulation. Acta Physiol Scand 160:123-132.

Berwick J, Martin C, Martindale J, Jones M, Johnston D, Zheng Y, Redgrave P, Mayhew J (2002) Hemodynamic response in the unanesthetized rat: intrinsic optical imaging and spectroscopy of the barrel cortex. J Cereb Blood Flow Metab 22:670-679.

Boas DA, Dale AM, Franceschini MA (2004) Diffuse optical imaging of brain activation: approaches to optimizing image sensitivity, resolution, and accuracy. Neuroimage 23 Suppl 1:S275-288.

Boas DA, Chen K, Grebert D, Franceschini MA (2004) Improving the diffuse optical imaging spatial resolution of the cerebral hemodynamic response to brain activation in humans. Opt Lett 29:1506-1508.

Boyden ES, Zhang F, Bamberg E, Nagel G, Deisseroth K (2005) Millisecond-timescale, genetically targeted optical control of neural activity. Nat Neurosci 8:1263-1268.

Buxton RB, Wong EC, Frank LR (1998) Dynamics of blood flow and oxygenation changes during brain activation: the balloon model. Magn Reson Med 39:855-864.

Cauli B, Tong XK, Rancillac A, Serluca N, Lambolez B, Rossier J, Hamel E (2004) Cortical GABA interneurons in neurovascular coupling: relays for subcortical vasoactive pathways. J Neurosci 24:8940-8949.

Chaigneau E, Oheim M, Audinat E, Charpak S (2003) Two-photon imaging of capillary blood flow in olfactory bulb glomeruli. Proc Natl Acad Sci U S A 100:13081-13086.

Chaigneau E, Tiret P, Lecoq J, Ducros M, Knopfel T, Charpak S (2007) The relationship between blood flow and neuronal activity in the rodent olfactory bulb. J Neurosci 27:6452-6460.

Chuquet J, Hollender L, Nimchinsky EA (2007) High-resolution in vivo imaging of the neurovascular unit during spreading depression. J Neurosci 27:4036-4044.

Davis TL, Kwong KK, Weisskoff RM, Rosen BR (1998) Calibrated functional MRI: mapping the dynamics of oxidative metabolism. Proc Natl Acad Sci U S A 95:1834-1839.

Denk W, Svoboda K (1997) Photon upmanship: why multiphoton imaging is more than a gimmick. Neuron 18:351-357.

Denk W, Strickler JH, Webb WW (1990) Two-photon laser scanning fluorescence microscopy. Science 248:73-76.

Devor A, Dunn AK, Andermann ML, Ulbert I, Boas DA, Dale AM (2003) Coupling of total hemoglobin concentration, oxygenation, and neural activity in rat somatosensory cortex. Neuron 39:353-359.

Devor A, Ulbert I, Dunn AK, Narayanan SN, Jones SR, Andermann ML, Boas DA, Dale AM (2005) Coupling of the cortical hemodynamic response to cortical and thalamic neuronal activity. Proc Natl Acad Sci U S A 102:3822-3827.

Devor A, Tian P, Nishimura N, Teng IC, Hillman EM, Narayanan SN, Ulbert I, Boas DA, Kleinfeld D, Dale AM (2007) Suppressed neuronal activity and concurrent arteriolar vasoconstriction may explain negative blood oxygenation level-dependent signal. J Neurosci 27:4452-4459.

Diez-Garcia J, Matsushita S, Mutoh H, Nakai J, Ohkura M, Yokoyama J, Dimitrov D, Knopfel T (2005) Activation of cerebellar parallel fibers monitored in transgenic mice expressing a fluorescent Ca2+ indicator protein. Eur J Neurosci 22:627-635.

Dirnagl U, Kaplan B, Jacewicz M, Pulsinelli W (1989) Continuous measurement of cerebral cortical blood flow by laser-Doppler flowmetry in a rat stroke model. J Cereb Blood Flow Metab 9:589-596.

Dirnagl U, Villringer A, Gebhardt R, Haberl RL, Schmiedek P, Einhaupl KM (1991) Three-dimensional reconstruction of the rat brain cortical microcirculation in vivo. J Cereb Blood Flow Metab 11:353-360.

Dunn AK, Bolay H, Moskowitz MA, Boas DA (2001) Dynamic imaging of cerebral blood flow using laser speckle. J Cereb Blood Flow Metab 21:195-201.

Dunn AK, Devor A, Dale AM, Boas DA (2005) Spatial extent of oxygen metabolism and hemodynamic changes during functional activation of the rat somatosensory cortex. Neuroimage 27:279-290.

Dunn AK, Devor A, Bolay H, Andermann ML, Moskowitz MA, Dale AM, Boas DA (2003) Simultaneous imaging of total cerebral hemoglobin concentration, oxygenation, and blood flow during functional activation. Opt Lett 28:28-30.

Faraci FM, Breese KR (1993) Nitric oxide mediates vasodilatation in response to activation of N-methyl-D-aspartate receptors in brain. Circ Res 72:476-480.

Filosa JA, Bonev AD, Nelson MT (2004) Calcium dynamics in cortical astrocytes and arterioles during neurovascular coupling. Circ Res 95:e73-81.

Filosa JA, Bonev AD, Straub SV, Meredith AL, Wilkerson MK, Aldrich RW, Nelson MT (2006) Local potassium signaling couples neuronal activity to vasodilation in the brain. Nat Neurosci.

Fox PT, Raichle ME (1986) Focal physiological uncoupling of cerebral blood flow and oxidative metabolism during somatosensory stimulation in human subjects. Proc Natl Acad Sci U S A 83:1140-1144.

Fox PT, Raichle ME, Mintun MA, Dence C (1988) Nonoxidative glucose consumption during focal physiologic neural activity. Science 241:462-464.

Garaschuk O, Milos RI, Konnerth A (2006) Targeted bulk-loading of fluorescent indicators for two-photon brain imaging in vivo. Nat Protoc 1:380-386.

Gobel W, Helmchen F (2007) New Angles on Neuronal Dendrites In Vivo. J Neurophysiol. 98:3770-3779.

Gobel W, Kampa BM, Helmchen F (2007) Imaging cellular network dynamics in three dimensions using fast 3D laser scanning. Nat Methods 4:73-79.

Grinvald A, Lieke E, Frostig RD, Gilbert CD, Wiesel TN (1986) Functional architecture of cortex revealed by optical imaging of intrinsic signals. Nature 324:361-364.

Hamel E (2004) Cholinergic modulation of the cortical microvascular bed. Prog Brain Res 145:171-178.

Hamel E (2006) Perivascular nerves and the regulation of cerebrovascular tone. J Appl Physiol 100:1059-1064.

Han X, Boyden ES (2007) Multiple-color optical activation, silencing, and desynchronization of neural activity, with single-spike temporal resolution. PLoS ONE 2:e299.

Harrison RV, Harel N, Kakigi A, Raveh E, Mount RJ (1998) Optical imaging of intrinsic signals in chinchilla auditory cortex. Audiol Neurootol 3:214-223.

Hillman EM, Boas DA, Dale AM, Dunn AK (2004) Laminar optical tomography: demonstration of millimeter-scale depth-resolved imaging in turbid media. Opt Lett 29:1650-1652.

Hillman EM, Devor A, Bouchard MB, Dunn AK, Krauss GW, Skoch J, Bacskai BJ, Dale AM, Boas DA (2007) Depth-resolved optical imaging and microscopy of vascular compartment dynamics during somatosensory stimulation. Neuroimage.

Hudetz AG (1997) Blood flow in the cerebral capillary network: a review emphasizing observations with intravital microscopy. Microcirculation 4:233-252.

Iadecola C (2004) Neurovascular regulation in the normal brain and in Alzheimer's disease. Nat Rev Neurosci 5:347-360.

Kleinfeld D, Friedman B, Lyden PD, Shih AY (2008) Targeted occlusion to surface and deep vessels in neocortex via linear and nonlinear optical absorption. In: Animal Models of Acute Neurological Injuries (Chen J, Xu Z, Xu X-M, Zhang J, eds): The Humana Press.

Kleinfeld D, Mitra PP, Helmchen F, Denk W (1998) Fluctuations and stimulus-induced changes in blood flow observed in individual capillaries in layers 2 through 4 of rat neocortex. Proc Natl Acad Sci U S A 95:15741-15746.

Kwong KK, Belliveau JW, Chesler DA, Goldberg IE, Weisskoff RM, Poncelet BP, Kennedy DN, Hoppel BE, Cohen MS, Turner R, et al. (1992) Dynamic magnetic resonance imaging of human brain activity during primary sensory stimulation. Proc Natl Acad Sci U S A 89:5675-5679.

Lauritzen M (2005) Opinion: Reading vascular changes in brain imaging: is dendritic calcium the key? Nat Rev Neurosci 6:77-85.

Lauritzen M, Fabricius M (1995) Real time laser-Doppler perfusion imaging of cortical spreading depression in rat neocortex. Neuroreport 6:1271-1273.

Malonek D, Grinvald A (1996) Interactions between electrical activity and cortical microcirculation revealed by imaging spectroscopy: implications for functional brain mapping. Science 272:551-554.

Mandeville JB, Marota JJ, Ayata C, Zaharchuk G, Moskowitz MA, Rosen BR, Weisskoff RM (1999) Evidence of a cerebrovascular postarteriole windkessel with delayed compliance. J Cereb Blood Flow Metab 19:679-689.

Martindale J, Mayhew J, Berwick J, Jones M, Martin C, Johnston D, Redgrave P, Zheng Y (2003) The hemodynamic impulse response to a single neural event. J Cereb Blood Flow Metab 23:546-555.

Mayhew J, Zhao L, Hou Y, Berwick J, Askew S, Zheng Y, Coffey P (1998) Spectroscopic investigation of reflectance changes in the barrel cortex following whisker stimulation. Adv Exp Med Biol 454:139-148.

Mulligan SJ, MacVicar BA (2004) Calcium transients in astrocyte endfeet cause cerebrovascular constrictions. Nature 431:195-199.

Nagel G, Szellas T, Huhn W, Kateriya S, Adeishvili N, Berthold P, Ollig D, Hegemann P, Bamberg E (2003) Channelrhodopsin-2, a directly light-gated cation-selective membrane channel. Proc Natl Acad Sci U S A 100:13940-13945.

Nemoto M, Sheth S, Guiou M, Pouratian N, Chen JW, Toga AW (2004) Functional signal- and paradigm-dependent linear relationships between synaptic activity and hemodynamic responses in rat somatosensory cortex. J Neurosci 24:3850-3861.

Nishimura N, Schaffer CB, Friedman B, Lyden PD, Kleinfeld D (2007) Penetrating arterioles are a bottleneck in the perfusion of neocortex. Proc Natl Acad Sci U S A.

Nishimura N, Schaffer CB, Friedman B, Tsai PS, Lyden PD, Kleinfeld D (2006) Targeted insult to subsurface cortical blood vessels using ultrashort laser pulses: three models of stroke. Nat Methods 3:99-108.

Obrig H, Villringer A (2003) Beyond the visible--imaging the human brain with light. J Cereb Blood Flow Metab 23:1-18.

Ogawa S, Tank DW, Menon R, Ellermann JM, Kim SG, Merkle H, Ugurbil K (1992) Intrinsic signal changes accompanying sensory stimulation: functional brain mapping with magnetic resonance imaging. Proc Natl Acad Sci U S A 89:5951-5955.

Ohki K, Chung S, Ch'ng YH, Kara P, Reid RC (2005) Functional imaging with cellular resolution reveals precise micro-architecture in visual cortex. Nature 433:597-603.

Peppiatt CM, Howarth C, Mobbs P, Attwell D (2006) Bidirectional control of CNS capillary diameter by pericytes. Nature 443:700-704.

Polimeni JR, Granquist-Fraser D, Wood RJ, Schwartz EL (2005) Physical limits to spatial resolution of optical recording: clarifying the spatial structure of cortical hypercolumns. Proc Natl Acad Sci U S A 102:4158-4163.

Raichle ME, Mintun MA (2006) Brain work and brain imaging. Annu Rev Neurosci 29:449-476.

Rancillac A, Rossier J, Guille M, Tong XK, Geoffroy H, Amatore C, Arbault S, Hamel E, Cauli B (2006) Glutamatergic control of microvascular tone by distinct GABA neurons in the cerebellum. J Neurosci 26:6997-7006.

Schaffer CB, Friedman B, Nishimura N, Schroeder LF, Tsai PS, Ebner FF, Lyden PD, Kleinfeld D (2006) Two-photon imaging of cortical surface microvessels reveals a robust redistribution in blood flow after vascular occlusion. PLoS Biol 4:e22.

Scremin OU (1995) Cerebral vascular system. In: The rat nervous system (Paxinos G, ed), pp 3-55. New York: Academic.

Sheth S, Nemoto M, Guiou M, Walker M, Pouratian N, Toga AW (2003) Evaluation of coupling between optical intrinsic signals and neuronal activity in rat somatosensory cortex. Neuroimage 19:884-894.

Sheth SA, Nemoto M, Guiou MW, Walker MA, Toga AW (2005) Spatiotemporal evolution of functional hemodynamic changes and their relationship to neuronal activity. J Cereb Blood Flow Metab 25:830-841.

Sheth SA, Nemoto M, Guiou M, Walker M, Pouratian N, Toga AW (2004) Linear and nonlinear relationships between neuronal activity, oxygen metabolism, and hemodynamic responses. Neuron 42:347-355.

Sheth SA, Nemoto M, Guiou M, Walker M, Pouratian N, Hageman N, Toga AW (2004) Columnar specificity of microvascular oxygenation and volume responses: implications for functional brain mapping. J Neurosci 24:634-641.

Sigler A, Goroshkov A, Murphy TH (2008) Hardware and methodology for targeting single brain arterioles for photothrombotic stroke on an upright microscope. J Neurosci Methods 170:35-44.

Simard M, Arcuino G, Takano T, Liu QS, Nedergaard M (2003) Signaling at the gliovascular interface. J Neurosci 23:9254-9262.

Sineshchekov OA, Jung KH, Spudich JL (2002) Two rhodopsins mediate phototaxis to low- and high-intensity light in Chlamydomonas reinhardtii. Proc Natl Acad Sci U S A 99:8689-8694.

Stosiek C, Garaschuk O, Holthoff K, Konnerth A (2003) In vivo two-photon calcium imaging of neuronal networks. Proc Natl Acad Sci U S A 100:7319-7324.

Svoboda K, Yasuda R (2006) Principles of two-photon excitation microscopy and its applications to neuroscience. Neuron 50:823-839.

Szobota S, Gorostiza P, Del Bene F, Wyart C, Fortin DL, Kolstad KD, Tulyathan O, Volgraf M, Numano R, Aaron HL, Scott EK, Kramer RH, Flannery J, Baier H, Trauner D, Isacoff EY (2007) Remote control of neuronal activity with a light-gated glutamate receptor. Neuron 54:535-545.

Takano T, Tian GF, Peng W, Lou N, Libionka W, Han X, Nedergaard M (2006) Astrocyte-mediated control of cerebral blood flow. Nat Neurosci 9:260-267.

Theer P, Hasan MT, Denk W (2003) Two-photon imaging to a depth of 1000 microm in living brains by use of a Ti:Al2O3 regenerative amplifier. Opt Lett 28:1022-1024.

Tsai PS, Nishimura N, Yoder EJ, White A, Dolnick E, Kleinfeld D (2002) Principles, design and construction of a two photon scanning microscope for in vitro and in vivo studies. In: Methods for In Vivo Optical Imaging (Frostig RD, ed), pp 113-171: CRC Press.

Tsai PS, Friedman B, Ifarraguerri AI, Thompson BD, Lev-Ram V, Schaffer CB, Xiong Q, Tsien RY, Squier JA, Kleinfeld D (2003) All-optical histology using ultrashort laser pulses. Neuron 39:27-41.

Vanzetta I, Grinvald A (1999) Increased cortical oxidative metabolism due to sensory stimulation: implications for functional brain imaging. Science 286:1555-1558.

Vanzetta I, Grinvald A (2001) Evidence and lack of evidence for the initial dip in the anesthetized rat: implications for human functional brain imaging. Neuroimage 13:959-967.

Vanzetta I, Hildesheim R, Grinvald A (2005) Compartment-resolved imaging of activity-dependent dynamics of cortical blood volume and oximetry. J Neurosci 25:2233-2244.

Villringer A, Planck J, Hock C, Schleinkofer L, Dirnagl U (1993) Near infrared spectroscopy (NIRS): a new tool to study hemodynamic changes during activation of brain function in human adults. Neurosci Lett 154:101-104.

Villringer A, Them A, Lindauer U, Einhaupl K, Dirnagl U (1994) Capillary perfusion of the rat brain cortex. An in vivo confocal microscopy study. Circ Res 75:55-62.

Volgraf M, Gorostiza P, Szobota S, Helix MR, Isacoff EY, Trauner D (2007) Reversibly caged glutamate: a photochromic agonist of ionotropic glutamate receptors. J Am Chem Soc 129:260-261.

Wayland H, Johnson PC (1967) Erythrocyte velocity measurement in microvessels by a two-slit photometric method. J Appl Physiol 22:333-337.

Zhang F, Wang LP, Brauner M, Liewald JF, Kay K, Watzke N, Wood PG, Bamberg E, Nagel G, Gottschalk A, Deisseroth K (2007) Multimodal fast optical interrogation of neural circuitry. Nature 446:633-639.

Zhang S, Murphy TH (2007) Imaging the impact of cortical microcirculation on synaptic structure and sensory-evoked hemodynamic responses in vivo. PLoS Biol 5:e119.

Zonta M, Angulo MC, Gobbo S, Rosengarten B, Hossmann KA, Pozzan T, Carmignoto G (2003) Neuron-to-astrocyte signaling is central to the dynamic control of brain microcirculation. Nat Neurosci 6:43-50.

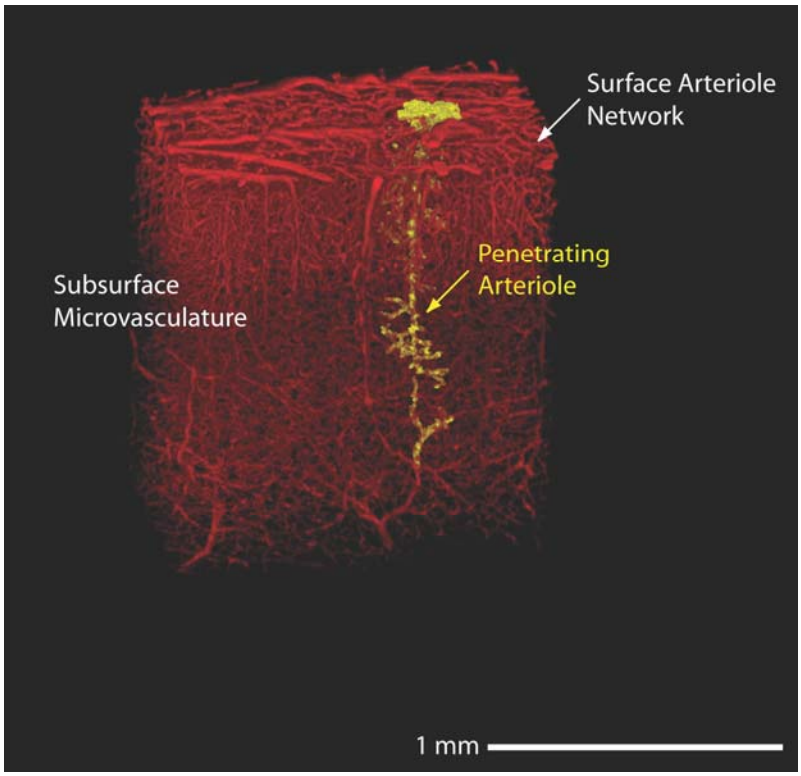
Surface Arteriole
Network
Penetrating
Arteriole
Subsurface
Microvasculature
1 mm

Figure 1

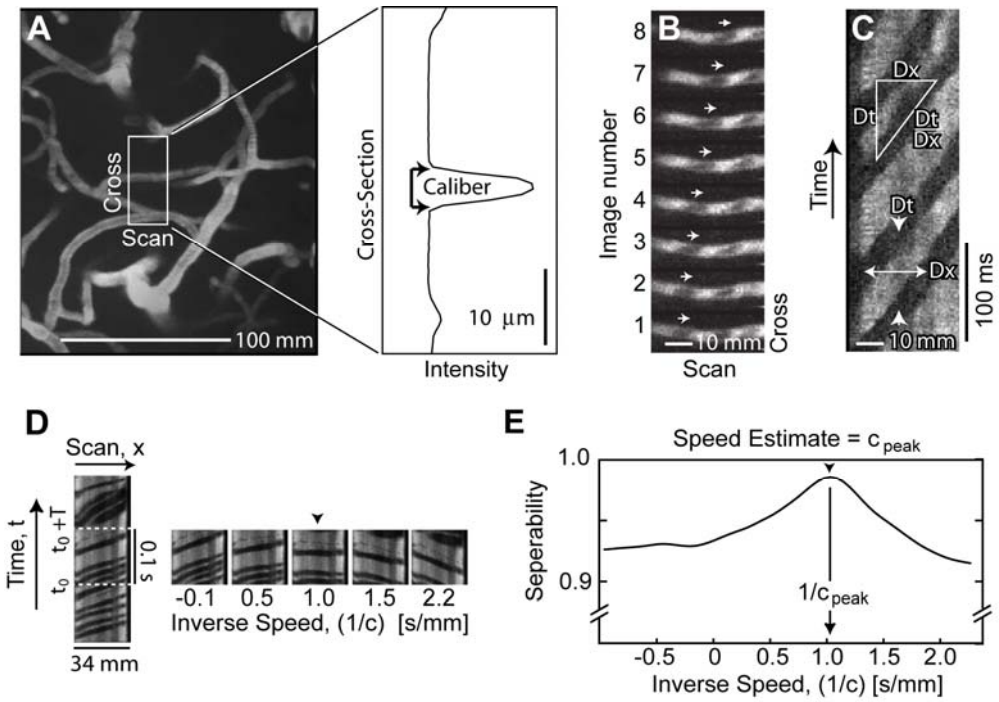
A
Cross
Scan
100 mm
Cross-Section
Caliber
10 µm
Intensity
B
Image number
8
7
6
5
4
3
2
1
10 mm
Cross
Scan
C
Dx
Dt
Dt
Dx
Time
Dt
Dx
100 ms
10 mm
D
Scan, x
Time, t
t_0+T
t_0
0.1 s
34 mm
-0.1 0.5 1.0 1.5 2.2
Inverse Speed, (1/c) [s/mm]
E
Speed Estimate = c_{peak}
1.0
0.9
Seperability
$1/c_{peak}$
-0.5 0 0.5 1.0 1.5 2.0
Inverse Speed, (1/c) [s/mm]

Figure 2

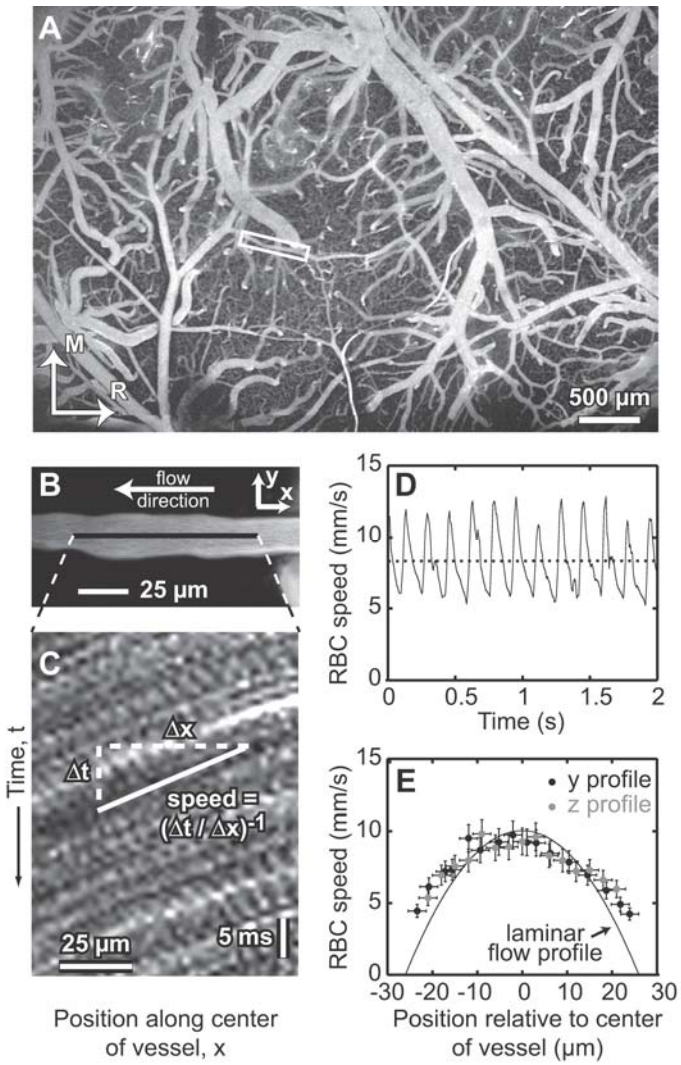
A
M
R
500 µm
B
flow direction
y
x
25 µm
C
Δx
Δt
speed = (Δt / Δx)-1
Time, t
25 µm
5 ms
Position along center of vessel, x
D
RBC speed (mm/s)
Time (s)
E
y profile
z profile
laminar flow profile
RBC speed (mm/s)
Position relative to center of vessel (µm)

Figure 3

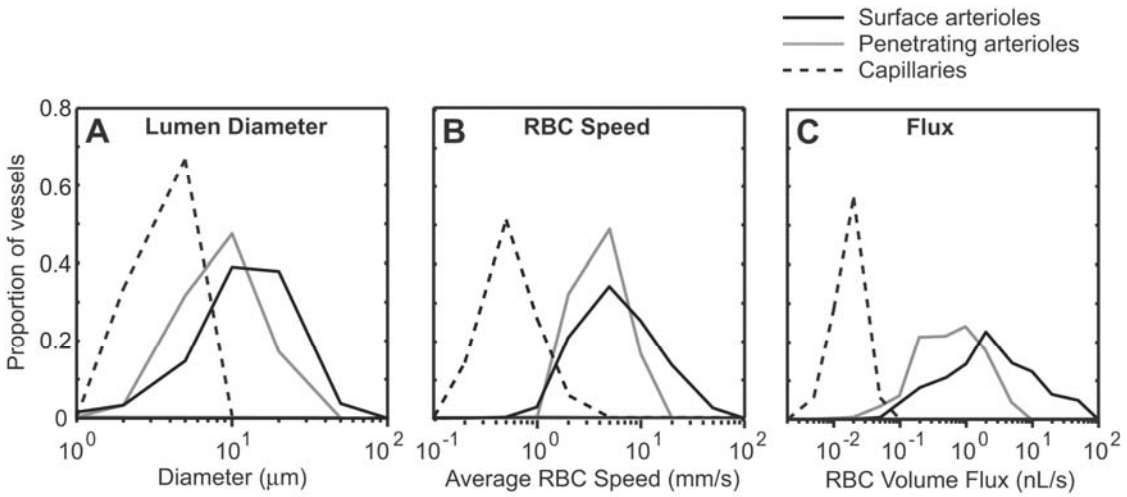
Surface arterioles
Penetrating arterioles
Capillaries
A
Lumen Diameter
B
RBC Speed
C
Flux
Proportion of vessels
0.8
0.6
0.4
0.2
0
10^0
10^1
10^2
Diameter (μm)
10^{-1}
10^0
10^1
10^2
Average RBC Speed (mm/s)
10^{-2}
10^{-1}
10^0
10^1
10^2
RBC Volume Flux (nL/s)

Figure 4

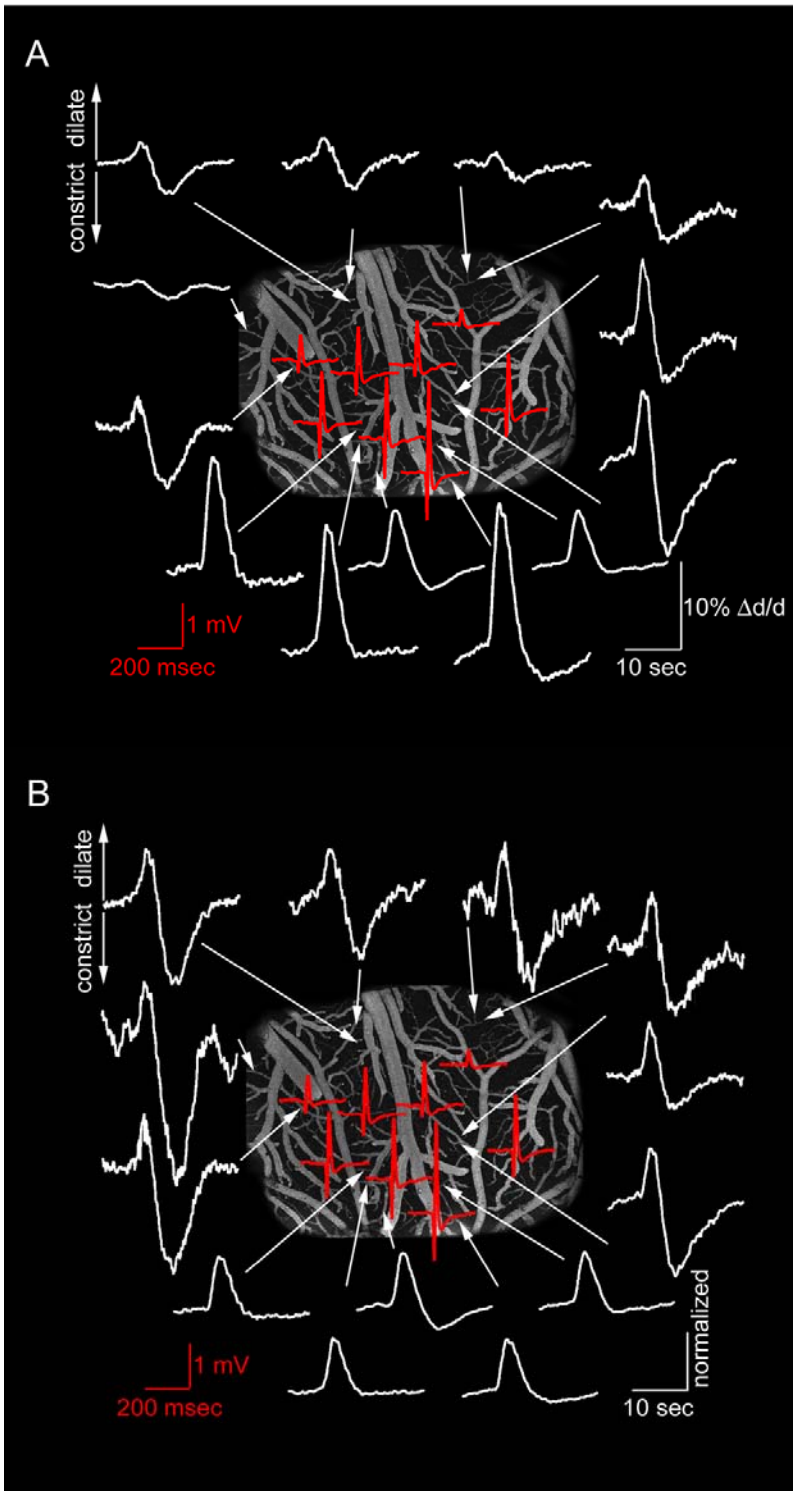
A
constrict dilate
1 mV
200 msec
10% Δd/d
10 sec
B
constrict dilate
1 mV
200 msec
normalized
10 sec

Figure 5

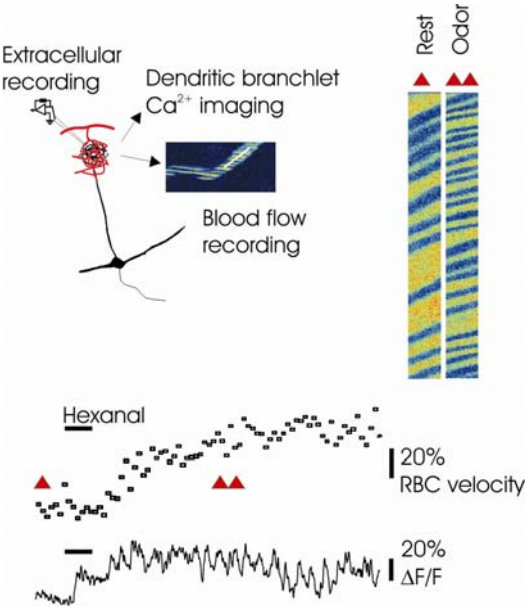
Extracellular recording
Dendritic branchlet
Ca2+ imaging
Blood flow recording
Rest
Odor
Hexanal
20%
RBC velocity
20%
ΔF/F

Figure 6

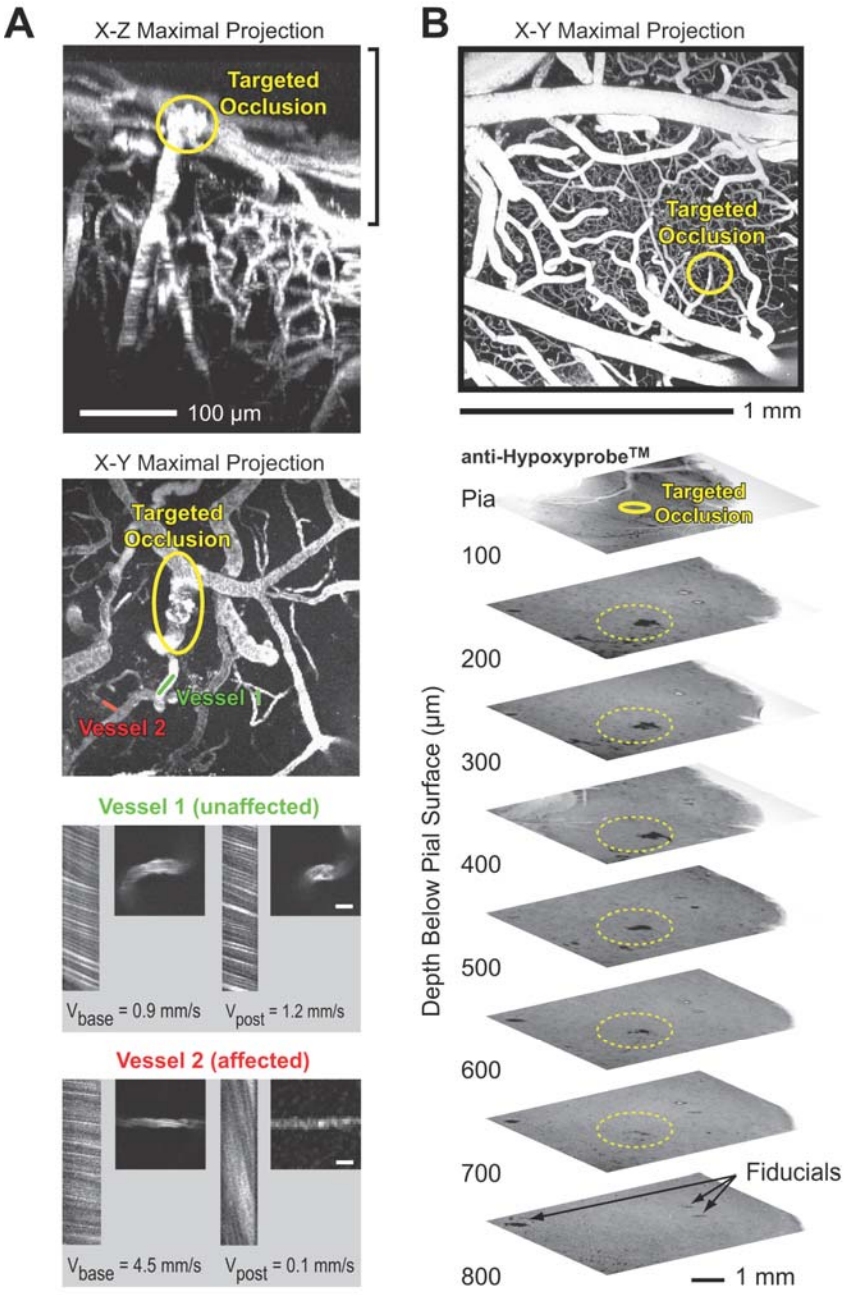
A
X-Z Maximal Projection
Targeted Occlusion
100 µm
X-Y Maximal Projection
Targeted Occlusion
Vessel 1
Vessel 2
Vessel 1 (unaffected)
V_{base} = 0.9 mm/s
V_{post} = 1.2 mm/s
Vessel 2 (affected)
V_{base} = 4.5 mm/s
V_{post} = 0.1 mm/s
B
X-Y Maximal Projection
Targeted Occlusion
1 mm
anti-Hypoxyprobe™
Pia
Targeted Occlusion
100
200
300
400
500
600
700
800
Depth Below Pial Surface (µm)
Fiducials
1 mm

Figure 7